Research Article | Vol. 27, No. 23 / 11 November 2019 / Optics Express 32892

Optics EXPRESS

Maintenance of broadband detection in photonic time-stretched coherent radar employing phase diversity

SITENG ZHANG, XING LI, JIANPING CHEN, AND WEIWEN ZOU*

State Key Laboratory of Advanced Optical Communication Systems and Networks, Intelligent Microwave Lightwave Integration Innovation Center (iMLic), Shanghai Jiao Tong University, Shanghai 200240, China
**wzou@sjtu.edu.cn*

Abstract: Frequency response fluctuation in a radar system distorts the envelope of the output signal after matched filtering, thereby impairing its broadband detection performance. Simulations are made under various types and degrees of fluctuation. The results prove that the peak power and range resolution of broadband detection suffer different levels of deterioration. Moreover, simulation results also show that two outputs with orthogonal phase diversity have complementary variation trends and their combination can effectively enhance the broadband detection performance. Based on theoretical analysis, we employ the combination of two orthogonal phase diversity to achieve broadband detection in the photonic time-stretched coherent radar. Compared with using an ordinary modulator, a dual-output-Mach-Zehnder-modulator-based system makes the dispersion-penalty-induced frequency response fluctuation decrease by 9.7 dB. For single target detection, the peak power is increased by 6.7 dB and the range resolution is improved from 8.4 cm to 4.8 cm. For two-target detection, a 6-cm spatial interval is distinguished reliably.

1. Introduction

For the next generation of radar systems, multiple functions are desired to acquire detailed information, such as target recognition, remote sensing, and imaging [1]. To meet such trends, microwave signals with high carrier frequency and wide bandwidth are introduced into radar systems [2]. However, a conventional microwave system always operates on specific narrowband and requires noisy up- and down-conversions, no matter achieved in digital or analog techniques [3,4]. Therefore, various photonics-based solutions were proposed to exploit the inherent advantages of photonics such as broadband, low loss, and low timing jitter [5–7]. In the pioneering demonstration [8], a photonics-based radar has proved its unique ability to compete with the conventional equivalent under the field test. However, the operating bandwidth is limited by the speed of digital processors [9,10]. To overcome this drawback, other photonics-based radar architectures were proposed and demonstrated [11–14]. All of them were working on the frequency modulated continuous wave (FMCW) mode and the broadband signal was achieved by frequency multiplication of the digital baseband signal. Unfortunately, the power conversion efficiency of a Mach-Zehnder modulator (MZM) is low and de-chirp technique will confine the maximum detection range due to large frequency deviation. Previously, we have proposed the photonic time-stretched coherent radar (PTS-CR) system [15]. It can generate broadband signals and alleviate processing pressure in the meanwhile. Broadband signal is achieved by beating two optical pulses with different dispersion values. The received echoes is time-stretched in advance to relieve the processing bandwidth demand. Moreover, we further improved the detection range and the signal-to-noise ratio of the system [16,17]. However, the frequency response is critical in a broadband radar system because the frequency response fluctuation distorts the output after matched filtering in the form of power loss and lobe modification [18]. In PTS-CR, the inherent

#370886 https://doi.org/10.1364/OE.27.032892
Journal © 2019 Received 24 Jun 2019; revised 15 Oct 2019; accepted 18 Oct 2019; published 28 Oct 2019

Optics EXPRESS

side effect known as dispersion penalty always accompanies with dispersive mediums, which causes frequency fluctuation [19,20]. Although single sideband (SSB) modulation can overcome dispersion penalty, microwave hybrid coupler will limit the working bandwidth [21]. Other methods based on dual-parallel modulators have also been reported [22,23], but extra bias or polarization stabilization is required, which increases system complexity.

In this paper, we employ a phase diversity scheme to maintain the broadband detection in PTS-CR. The output after matched filter is simulated under various types and degrees of fluctuation. The deterioration of peak power and range resolution for broadband detection is analyzed. Thanks to the phase diversity, two orthogonal outputs have complementary variation trends and their combination effectively maintains the broadband detection performance. Experiments are conducted to demonstrate the broadband detection ability. Broadband signal is still generated by the optical heterodyne interference [15]. The echoes are modulated by a dual-output Mach-Zehnder modulator (DO-MZM) and then time-stretched fourfold. The two outputs with the orthogonal phase diversity are combined to achieve broadband detection. Experimental results show that the frequency response fluctuation is decreased by 9.7 dB. For single target detection, the peak power is increased by 6.7 dB and the range resolution is 4.8 cm. For two targets detection, distance of 6 cm can be distinguished reliably.

2. Theoretical analysis and simulation

To achieve high peak power and narrow range resolution, broadband signals are used in radar systems. An ideal linear frequency modulated (LFM) microwave signal can be expressed as

$$S_{ideal}(t) = A\cos(2\pi f_0 t + \pi k t^2) \quad |t| \le T/2 \tag{1}$$

where A, f_0, k, and T represent the amplitude, carrier frequency, frequency modulated rate, and duration of $S_{ideal}(t)$, respectively. The envelope of the convolutional output after matched filtering is given as

$$E_{ideal}(t) = S_{ideal}(t) \otimes S_{ideal}{}^{*}(-t) = \sqrt{BT}[(\sin \pi Bt)/(\pi Bt)] \tag{2}$$

where $B = kT$ is the bandwidth of $S_{ideal}(t)$ and $\otimes$ denotes the convolution operator. The temporal width of the pulse $E_{ideal}(t)$ is $1/B$ and the peak power is $\sqrt{BT}$. However, there always exists fluctuation on the frequency response in practical applications. The practical envelope can be expressed as

$$E(t) = S(t) \otimes S^{*}(t) = P[(\sin \pi B_{equ} t) \Big/ \pi B_{equ} t] \tag{3}$$

where $S(t)$ represents the practical signal, P represents the peak power, and B_{equ} represents the equivalent bandwidth. Two key parameters can be used to evaluate the broadband detection performance, which are the peak power P and the range resolution $D = c \Big/ (2B_{equ})$.

Suppose the frequency response has a cosine-like expression as $H(f) = \cos(\phi(f)) = \cos(\phi_0 + a(f - f_{\min})^b)$, where $a>0, b>0$. The maximum phase deviation is expressed as $\Delta\phi = \mathrm{a}(f_{\max} - f_{\min})^b$. A unit LFM signal covering the whole X band (from 8 GHz to 12 GHz) is supposed to be the ideal signal. The temporal duration is set to be $T = 2$ ns. The outputs after matched filtering under four different types of fluctuation such as (1) $\phi_0 = 0°, b = 1$, (2) $\phi_0 = 90°, b = 1$, (3) $\phi_0 = 0°, b = 2$ and (4) $\phi_0 = 90°, b = 2$ are simulated. Note that the orthogonal phase diversity is the complementary phase difference, such as (1) versus (2) or (3) versus (4). The corresponding peak power loss $L_P = P \Big/ \sqrt{BT}$ and range resolution D versus the maximum phase deviation $\Delta\phi$ are simulated, which are depicted in Fig. 1(a)– 1(d).

It can be seen from Fig. 1 that the peak power loss and the range resolution have opposite variation trends. It means that the fluctuation leads to deterioration of both power and bandwidth, thus impairing the broadband detection performance. In addition, the results with orthogonal phase diversity [see Fig. 1(a) and Fig. 1(b)] are in a complementary variation trend under the same

Optics EXPRESS

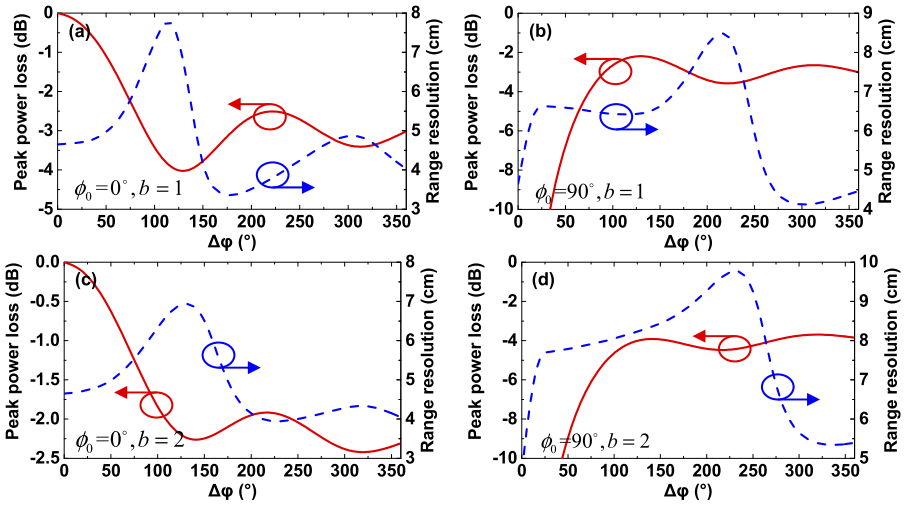

Fig. 1. Simulation results of the peak power loss and range resolution versus the maximum phase deviation under different types of fluctuation: (a) $\phi_0 = 0°, b = 1$, (b) $\phi_0 = 90°, b = 1$, (c) $\phi_0 = 0°, b = 2$, and (d) $\phi_0 = 90°, b = 2$. Solid line: peak power loss; dashed line: range resolution.

type of fluctuation. Therefore, the envelopes with orthogonal phase diversity can be combined to maintain the broadband detection performance.

To verify the validity, two simulated outputs with the orthogonal phase diversity such as (3) $\phi_0 = 0°, b = 2$ and (4) $\phi_0 = 90°, b = 2$ are combined at different ratios of y/x. Note that the parameters of x and y determines the combined envelope of $E_{comb}(t) = x^2 \cdot E_3(t) + y^2 \cdot E_4(t)$, where $E_3(t)$ and $E_4(t)$ are the outputs of the simulation condition (3) and (4), respectively. We simulate the peak power loss and range resolution versus the maximum phase deviation again, which are depicted in Fig. 2. The simulation results prove that the combination can effectively suppress the negative effect of frequency response fluctuation. When $y/x = 1$, the radar system can maintain the broadband detection performance perfectly.

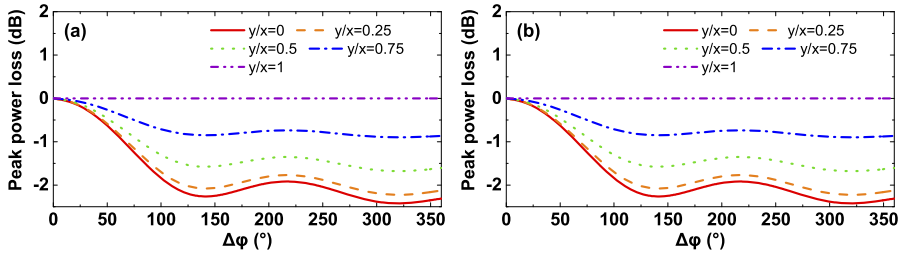

Fig. 2. Simulation results of (a) peak power loss and (b) effective range resolution versus the maximum phase deviation with different combination ratios of y/x.

In PTS-CR, it is inevitable to use the second dispersive medium to achieve time stretch in the receiver. After modulation, the sidebands accumulate different phases when propagating in the second dispersive medium. The phase can be written as $\phi(f) = \pm(2\pi f)^2\beta_2 L$ [20], where f is the frequency of the microwave signal and $\beta_2 L$ is the dispersion value of the second dispersive medium. The specific expression of dispersion-penalty-induced frequency response can be

Optics EXPRESS

described as [19]

$$H_{dp}(f) = [\cos(2\pi^2\beta_2 L_2 f^2 \Big/ M)]^2 \tag{4}$$

where $M = 1 + L_2/L_1$ is the time stretch factor and L_1, L_2 are the lengths of the first and second dispersive mediums. Since the optical chirped carrier makes less influence [24], the LFM signal in the receiver can be deduced as

$$S_{dp}(t) = \cos[2\pi(f_0 t + kt^2 \Big/ 2) \Big/ M] \cos[2\pi^2 L_2\beta_2(f_0 + kt)^2 \Big/ M] \text{ , } -T/2 \le t \le T/2 \tag{5}$$

The first cosine term is the LFM signal which has been slowed down M times. The second cosine term represents the distortion caused by the dispersion-penalty-induced frequency response.

3. Experimental results

3.1. Experimental setup and measurements

The PTS-CR system employing DO-MZM is shown in Fig. 3. Since the outputs of DO-MZM have orthogonal phase diversity [25], the combination of dual outputs can be used to maintain the broadband detection performance. A passive mode-locked fiber laser (MLL, Menlo Systems, C-Fiber) with a pulse repetition rate of 100 MHz is chosen as the optical source. The transmitter and the receiver share the optical power equally by a 50:50 optical coupler (OC1). In the transmitter, optical pulses from one branch of OC1 are extended in time domain by a dispersion compensation fiber (DCF1) and then filtered by a tunable optical filter (TOF1, Alnair Labs, CVF-300CL). The dispersion value of DCF1 is 1263.5 ps^2 (OFS, DCM-60-C) and the volume is 26.5*23.5*4.5 cm. The filter bandwidth of TOF1 is 2 nm. An erbium-doped fiber amplifier (EDFA1) is used to compensate the propagation loss. Then the optical path is split into two arms by OC2. In the upper arm, DCF2 adds an extra dispersion value of 29.5 ps^2. In the lower arm, a variable optical delay line (VODL, General Photonics, MDL-002) is embedded to generate specific carrier frequency. A polarization controller (PC1) is used to increase the interference visibility. The optical pulses from two arms are coupled by OC3 and converted by a photo-detector (PD1) with 18 GHz bandwidth to generate LFM microwave signals. After amplified by an electric amplifier (AMP1, RF Bay, LNA-14G), the LFM signals are transmitted by the antenna (TA). In the receiver, the echoes are received by another antenna (RA) and amplified by AMP2 (RF Bay, LNA-14G). The optical pulses from the other branch of OC1 are filtered by TOF2 (Alnair Labs, CVF-220CL) with a bandwidth of 4 nm and dispersed by DCF3 with a dispersion value of 846.9 ps^2 (OFS, DCM-40-C). Then the optical pulses are modulated with the echoes in a DO-MZM (EOSPACE, AZ-1*2-AV5-40). After modulation, two outputs of the DO-MZM enter two separate optical circulators (CIR1 and CIR2) and propagate through DCF4 in opposite direction (a and b). To achieve a time stretched factor of 4, the dispersion value of DCF4 is 2553.2 ps^2. It consists of two sections of dispersive compensation fibers (OFS, DCM-60-C). EDFA3 and EDFA4 (Calmar, Coronado) are incorporated in two channels. Finally, they outputs are detected by a balanced photodetector (BPD, DSC-R412). It is noted that the lengths of the separate paths from DO-MZM to BPD are aligned. The outputs from BPD are captured and recorded by the oscilloscope (OSC, Lecroy, SDA 845Zi-A).

To testify the broadband detection performance, the frequency response of the radar system is measured by a Vector Network Analyzer (VNA, Agilent, PNA-X N5247A). The experimental setup is depicted in Fig. 4(a). MLL is replaced by a continuous wave laser (Alnair Labs, TLG-200) at 1550 nm to avoid the influence of time stretch. DCF4 is replaced with a short fiber to measure the relative delay between the paths from DO-MZM to BPD. Figure 4(b) reveals that the two paths are perfectly aligned with an error of 10 ps.

The frequency response is also measured when DCF4 is incorporated into the system. Figure 5(a) shows the theoretical results by Eq. (4) and Fig. 5(b) illustrates the experimental

Optics EXPRESS

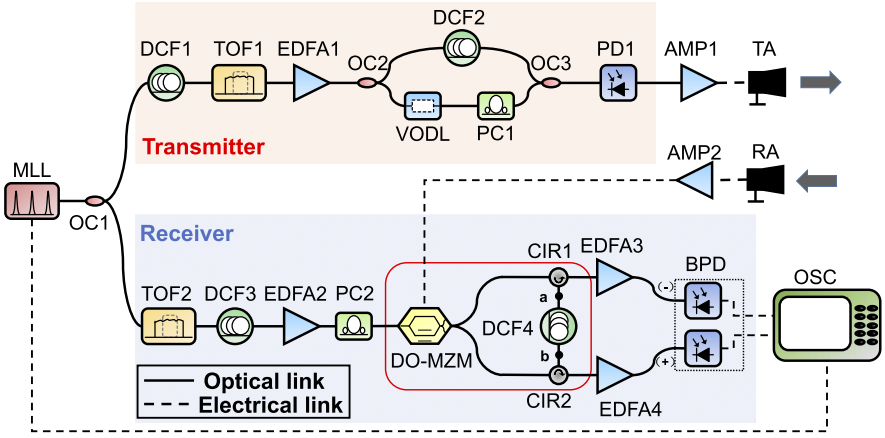

Fig. 3. Experimental setup of the PTS-CR employing phase diversity. MLL: mode-locked laser; OC: optical coupler; DCF: dispersion compensation fiber; TOF: tunable optical filter; EDFA: erbium-doped fiber amplifier; VODL: variable optical delay line; PC: polarization controller; PD: photodetector; AMP: amplifier; TA: transmitting antenna; RA: receiving antenna; DO-MZM: dual-output Mach-Zehnder modulator; CIR: circulator; BPD: balanced photodetector; OSC: oscilloscope.

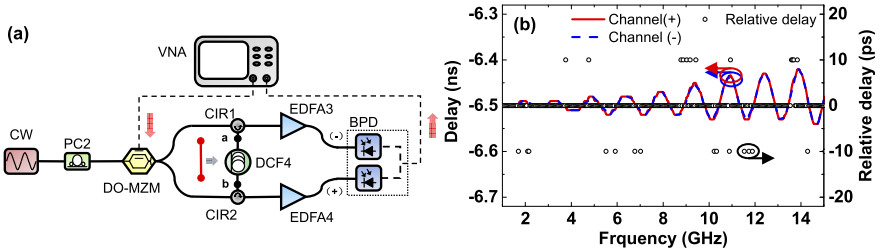

Fig. 4. (a) Experimental setup for the frequency response of the system. CW: continuous wave laser, VNA: vector network analyzer. (b) Measured time delay of the paths from DO-MZM to BPD and the relative delay between the paths. Solid line: Channel (+); dashed line: Channel (-).

results of the two channels. The experimental results are in good agreement with the simulation results. It reveals that the two channels have complementary variation trends and the fluctuation is improved from 12.3 dB to 2.6 dB by combination.

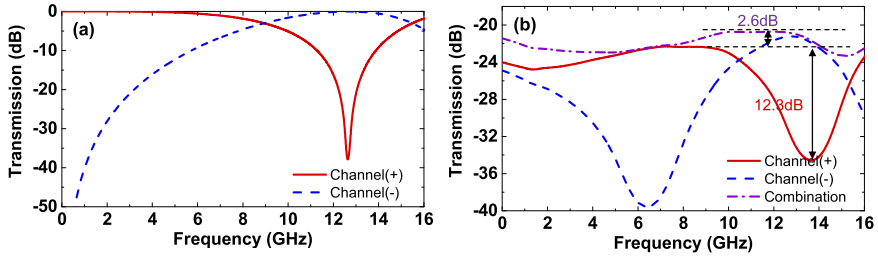

Fig. 5. (a) Theoretical and (b) experimental results of the frequency response of the two channels. Solid line: Channel (+); dashed line: Channel (-); dashed dotted line: combination.

Optics EXPRESS

3.2. Target-detection experimental results

The target-detection experiments are carried out. The output in Channel (+) and the combined output are compared to prove the broadband detection ability. Figures 6(a) and 6(b) show the temporal plot and the short-time Fourier transform (STFT) of the generated LFM signal, respectively. The duration is approximately 2 ns, which is consistent with the theoretical value of 1.97 ns. The amplitude is almost even along the whole duration. The temporal plot and STFT of the received LFM signal in Channel (+) after transmission and time stretch are depicted in Figs. 6(c) and 6(d), respectively. The duration is approximately 8 ns, corresponding to a time stretched factor of 4. It can be seen that the amplitude is seriously affected by the frequency response fluctuation induced by dispersion penalty.

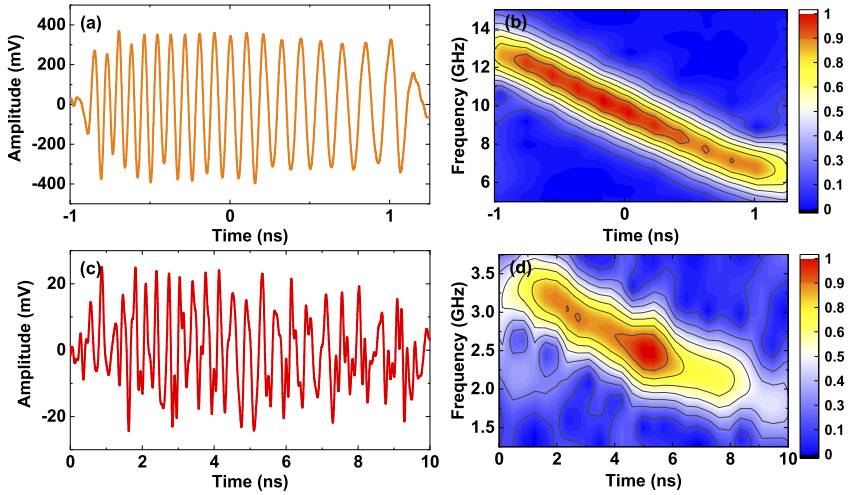

Fig. 6. (a) The temporal plot and (b) the short-time Fourier transform (STFT) of the generated LFM signal; (c) the temporal plot and (d) the short-time Fourier transform (STFT) of the received LFM signal in Channel (+).

The envelopes of the outputs after the matched filtering [15] are depicted in Fig. 7. Simulation results [Fig. 7(a)] indicates that the peak power loss is 8.2 dB and the range resolution is 8 cm in Channel (+) whereas the experimental results [Fig. 7(b)] are 6.7 dB and 8.4 cm, respectively. Due to the dispersion-penalty-induced fluctuation, the equivalent bandwidth is decreased by 42.5%. Simulation results reveal that the combined outputs are close to the ideal situation. The experimental result shows that the range resolution is enhanced to 4.8 cm by the combination of two channels, which is consistent with the simulation result of 4.6 cm. It is confirmed that the combined outputs employing the orthogonal phase diversity can effectively maintain the broadband detection ability.

Furthermore, two identical thin metal flats with the size of 10 cm ×15 cm are used for target distinction. The targets are placed ~70 cm away from the antennas and ~6 cm away from each other, as shown in Fig. 8(a). The envelopes of the outputs after the matched filtering are shown in Fig. 8(b). From the outputs of Channel (+), two targets are difficult to be distinguished because of the fake peak caused by the superposition of the side lobes or the dispersion penalty in the receiver. However, the two targets can be distinguished reliably from the combined outputs due to the maintenance of the broadband detection ability.

Optics EXPRESS

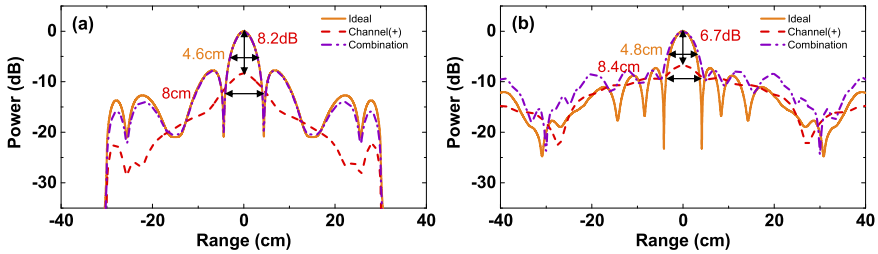

Fig. 7. The envelopes of the outputs after matched filtering (a) in simulation and (b) in experiment (solid line: ideal situation; dashed line: Channel (+); dashed dotted line: combination).

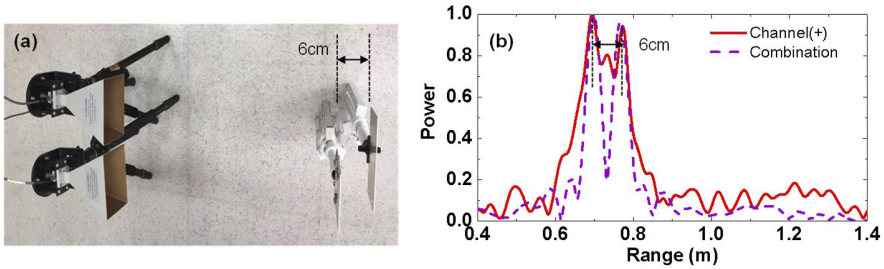

Fig. 8. (a) Configuration of the antennas and targets and (b) the envelopes of the outputs after the matched filtering process in Channel (+) (solid) and the combined outputs (dashed).

4. Conclusions

We have employed a phase diversity scheme to maintain the broadband detection in PTS-CR. As two key parameters for broadband detection, the peak power and range resolution are simulated and measured to evaluate the performance. Experimental results prove that the frequency response fluctuation has been reduced by 9.7 dB. For single target detection, the peak power has increased by 6.7 dB and the range resolution is 4.8 cm, which is close to the ideal situation. For two targets detection, distance of 6 cm can be distinguished reliably. The proposed radar architecture shows its potential to operate at any desired frequency band to meet the demands of multiband and broadband.

Funding

National Natural Science Foundation of China (61535006, 61571292, 61822508).

References

1. W. L. Melvin and J. A. Scheer, *Principles of Modern Radar: Vol. II Advanced Techniques* (SciTech Publishing, 2012).
2. J. D. McKinney, "Technology: Photonics illuminates the future of radar," Nature **507**(7492), 310–312 (2014).
3. J. Capmany and D. Novak, "Microwave photonics combines two worlds," Nat. Photonics **1**(6), 319–330 (2007).
4. P. Ghelfi, F. Laghezza, F. Scotti, G. Serafino, S. Pinna, D. Onori, E. Lazzeri, and A. Bogoni, "Photonics in Radar Systems: RF Integration for State-of-the-Art Functionality," IEEE Microw. Mag. **16**(8), 74–83 (2015).
5. G. C. Valley, "Photonic analog-to-digital converters," Opt. Express **15**(5), 1955–1982 (2007).
6. J. Yao, "Microwave photonics," J. Lightwave Technol. **27**(3), 314–335 (2009).
7. T. R. Clark and R. Waterhouse, "Photonics for RF Front Ends," IEEE Microw. Mag. **12**(3), 87–95 (2011).
8. P. Ghelfi, F. Laghezza, F. Scotti, G. Serafino, A. Capria, S. Pinna, D. Onori, C. Porzi, M. Scaffardi, A. Malacarne, V. Vercesi, E. Lazzeri, F. Berizzi, and A. Bogoni, "A fully photonics-based coherent radar system," Nature **507**(7492), 341–345 (2014).
9. S. Xu, W. Zou, G. Yang, and J. Chen, "Ultra-high range resolution demonstration of a photonics-based microwave radar using high-repetition-rate mode-locked fiber laser," Chin. Opt. Lett. **16**(6), 062801 (2018).

Optics EXPRESS

10. J. Yang, S. Li, X. Xiao, D. Wu, X. Xue, and X. Zheng, "Broadband photonic ADC for microwave photonics-based radar receiver," Chin. Opt. Lett. **16**(6), 060605 (2018).
11. R. Li, W. Li, M. Ding, Z. Wen, Y. Li, L. Zhou, S. Yu, T. Xing, B. Gao, Y. Luan, Y. Zhu, P. Guo, Y. Tian, and X. Liang, "Demonstration of a microwave photonic synthetic aperture radar based on photonic-assisted signal generation and stretch processing," Opt. Express **25**(13), 14334–14340 (2017).
12. F. Zhang, Q. Guo, Z. Wang, P. Zhou, G. Zhang, J. Sun, and S. Pan, "Photonics-based broadband radar for high-resolution and real-time inverse synthetic aperture imaging," Opt. Express **25**(14), 16274–16281 (2017).
13. S. Peng, S. Li, X. Xue, X. Xiao, D. Wu, X. Zheng, and B. Zhou, "High-resolution W-band ISAR imaging system utilizing a logic-operation-based photonic digital-to-analog converter," Opt. Express **26**(2), 1978–1987 (2018).
14. A. Wang, J. Wo, X. Luo, Y. Wang, W. Cong, P. Du, J. Zhang, B. Zhao, J. Zhang, Y. Zhu, J. Lan, and L. Yu, "Ka-band microwave photonic ultra-wideband imaging radar for capturing quantitative target information," Opt. Express **26**(16), 20708–20717 (2018).
15. W. Zou, H. Zhang, X. Long, S. Zhang, Y. Cui, and J. Chen, "All-optical central-frequency-programmable and bandwidth-tailorable radar," Sci. Rep. **6**(1), 19786 (2016).
16. S. Zhang, W. Zou, N. Qian, and J. Chen, "Enlarged Range and Filter-Tuned Reception in Photonic Time-Stretched Microwave Radar," IEEE Photonics Technol. Lett. **30**(11), 1028–1031 (2018).
17. N. Qian, W. Zou, S. Zhang, and J. Chen, "Signal-to-noise ratio improvement of photonic time-stretch coherent radar enabling high-sensitivity ultrabroad W-band operation," Opt. Lett. **43**(23), 5869–5872 (2018).
18. M. C. Leifer and R. L. Haupt, "Power amplifier and power supply distortion of pulse compression radar chirps," in *Proceedings of Radar Conference*, (IEEE, 2016), pp. 1–4.
19. F. Coppinger, A. S. Bhushan, and B. Jalali, "Photonic time stretch and its application to analog-to-digital conversion," IEEE Trans. Microwave Theory Tech. **47**(7), 1309–1314 (1999).
20. Y. Han and B. Jalali, "Photonic time-stretched analog-to-digital converter: fundamental concepts and practical considerations," J. Lightwave Technol. **21**(12), 3085–3103 (2003).
21. J. M. Fuster, D. Novak, A. Nirmalathas, and J. Marti, "Single-sideband modulation in photonic time-stretch analogue-to-digital conversion," Electron. Lett. **37**(1), 67–68 (2001).
22. S. Li, X. Zheng, H. Zhang, and B. Zhou, "Compensation of dispersion-induced power fading for highly linear radio-over-fiber link using carrier phase-shifted double sideband modulation," Opt. Lett. **36**(4), 546–548 (2011).
23. S. Zhu, M. Li, N. Zhu, and W. Li, "Transmission of dual-chirp microwave waveform over fiber with compensation of dispersion-induced power fading," Opt. Lett. **43**(11), 2466–2469 (2018).
24. S. Dubovitsky, W. H. Steier, S. Yegnanarayanan, and B. Jalali, "Analysis and improvement of Mach-Zehnder modulator linearity performance for chirped and tunable optical carriers," J. Lightwave Technol. **20**(5), 886–891 (2002).
25. Y. Han, O. Boyraz, and B. Jalali, "Ultrawide-band photonic time-stretch a/D converter employing phase diversity," IEEE Trans. Microwave Theory Tech. **53**(4), 1404–1408 (2005).